atmosphere

MDPI

Article

Intertropical Convergence Zone as the Possible Source Mechanism for Southward Propagating Medium-Scale Traveling Ionospheric Disturbances over South American Low-Latitude and Equatorial Region

Patrick Essien [1,2,3], Cosme Alexandre Oliveira Barros Figueiredo [3], Hisao Takahashi [3], Nana Ama Browne Klutse [2,4,*], Cristiano Max Wrasse [3], João Maria de Sousa Afonso [5], David Pareja Quispe [6], Solomon Otoo Lomotey [3,7], Tunde Toyese Ayorinde [3], José H. A. Sobral [3], Moses Jojo Eghan [1], Samuel Sanko Sackey [1], Diego Barros [3], Anderson V. Bilibio [3], Francis Nkrumah [1,2] and Kwesi Akumenyi Quagraine [1]

1 Meteorology and Atmospheric Research Lab, Department of Physics, School of Physical Sciences, College of Agriculture and Natural Sciences, University of Cape Coast, Cape Coast PMB TF0494, Ghana
2 Climate Change Science, African Institute for Mathematical Sciences (AIMS) Rwanda, Kigali 20093, Rwanda
3 Space Weather Division, National Institute for Space Research (INPE), Av. dos Astronautas, Sao Jose dos Campos 12227-010, SP, Brazil
4 Department of Physics, University of Ghana, Accra 00233, Ghana
5 National Institute of Meteorology and Geophysics of Angola (INAMET), 21 de Janeiro Street, Morro Bento Neighborhood, Luanda, Angola
6 Departamento de Física Interdisciplinaria, Facultad de Ciencias Físicas, Universidad Nacional Mayor de San Marcos (UNMSM), Av. Carlos Germán Amezaga, No. 375, Cercado de Lima 15081, Peru
7 Department of Smart Technologies, School of Built Environment (SBE), University of Environment and Sustainable Development (UESD), Somanya ACT 898, Ghana
* Correspondence: nklutse@ug.edu.gh or nana.klutse@aims.ac.rw; Tel.: +233-24-498-3637

Abstract: This paper presents the Intertropical Convergence Zone (ITCZ) as the possible source mechanism of the medium-scale traveling ionospheric disturbances (MSTIDs) propagating to the southeast direction over the South American region. Using the data collected by the GNSS dual-frequency receivers network from January 2014 to December 2019, detrended TEC maps were generated to identify and characterize 144 MSTIDs propagating southeastward over the South American low-latitude and equatorial region. We also used images from the Geostationary Operational Environmental Satellite (GOES) 13 and 16 in the infrared (IR) and water vapor (WV) channel, and reanalisys data from the National Centers for Environmental Prediction (NCEP) of the National Oceanic and Atmospheric Administration (NOAA) to study the daily features and seasonal migration of ITCZ. In the winter, when ITCZ migrates to the northern hemisphere around 10–15° N, 20 MSTIDs propagated southeastward. During summer, when the ITCZ lies within the continent, around 0–5° S 80 MSTIDs were observed to propagate southeastward; in the equinoxes (spring and fall), 44 MSTIDs were observed. Again, the MSTIDs propagating southeastward showed a clear seasonality of their local time dependence; in summer, the MSTIDs occurred frequently in the evening hours, whereas those in winter occurred during the daytime. We also found for the first time that the day-to-day observation of ITCZ position and MSTIDs propagation directions were consistent. With regard to these new findings, we report that the MSTIDs propagating southeastward over the South American region are possibly induced by the atmospheric gravity waves, which are proposed as being generated by the ITCZ in the troposphere. The mean distribution of the horizontal wavelength, period, and phase velocity are 698 ± 124 km, 38 ± 8 min, and 299 ± 89 m s^{-1}, respectively. For the first time, we were able to use MSTID propagation directions as a proxy to study the source region.

Keywords: ITCZ; gravity waves; MSTIDs; ionosphere

Citation: Essien, P.; Figueiredo, C.A.O.B.; Takahashi, H.; Klutse, N.A.B.; Wrasse, C.M.; Afonso, J.M.d.S.; Quispe, D.P.; Lomotey, S.O.; Ayorinde, T.T.; Sobral, J.H.A.; et al. Intertropical Convergence Zone as the Possible Source Mechanism for Southward Propagating Medium-Scale Traveling Ionospheric Disturbances over South American Low-Latitude and Equatorial Region. *Atmosphere* **2022**, *13*, 1836. https://doi.org/10.3390/atmos13111836

Academic Editors: Stefan Bender, Yvan Orsolini and Kristell Pérot

Received: 12 September 2022
Accepted: 28 October 2022
Published: 4 November 2022

1. Introduction

The Earth's ionosphere is largely impacted by solar and magnetic activities; however, many studies have reported that severe tropospheric weather events, earthquakes, tsunamis, volcanic eruptions, and human-made events such as explosions, rocket and missile launches, and microblasts among others [1] from below, can also affect ionosphere triggering irregularities [2,3]. These disturbances from below propagate in the ionospheric plasma as gravity waves (internal or acoustic), causing traveling Ionospheric disturbances (TIDs), which might induce further irregularities such as equatorial plasma bubbles (EPBs) in the equatorial region. The upward propagation of gravity waves triggers the significant increase in amplitude due to the exponential decrease in the atmospheric density with increasing altitude. The gravity waves generated in the neutral atmosphere may consequently produce significant disturbances in the upper atmosphere and ionosphere, which can be detected by ionospheric sounding tools, such as Global Navigation Satellite System (GNSS) receivers, ionosondes, and all-sky cameras, among others.

The study of TID commenced with long-distance radio transmission, considering, variations and interruptions in over-the-horizon transmissions [4]. The pioneering paper published by Hines [5] proposed that TIDs are caused by upward propagating gravity wave disturbances originating from the neutral atmosphere (e.g., troposphere). The gravity-wave–MSTID transfer function depends on characteristics such as period, phase velocity, horizontal wavelength, wavenumber, amplitude, and propagation direction of the wave in question, in addition to the conditions in the neutral atmosphere and ionosphere [6,7]. Refs. Tsunoda [8], Su et al. [9] reported that mesoscale convective systems are usually found within the intertropical convergence zone (ITCZ), and equatorial spread morphology is assumed to be controlled by the seasonal migration of gravity waves generated by the ITCZ. Thus, the call for the investigation of the origin of the present equatorial MSTIDs from the neutral atmosphere and other geophysical sources in relation to the statistical behavior is important.

In the middle latitudes, day- and nighttime MSTIDs have been reported to be generated via atmospheric gravity waves propagating in the F-layer bottom height [10–13] and Perkins instability [14–16], while at high latitudes, MSTIDs have been attributed to the geomagnetic storms and polar electroject [17]. Several authors have suggested that the possible source regions for equatorial and low-latitude MSTIDs, especially those propagating southeastward, are linked to the gravity waves in the thermosphere that originate from the ITCZ [10,18–20]. Knowing and understanding the sources of MSTIDs is of utmost importance for unraveling the complexities of the neutral atmosphere and ionosphere coupling and, eventually, the prediction of the climatology of the occurrence of MSTIDs in the future.

The importance of the primary sources of MSTIDs over the low-latitude and equatorial ionosphere can not be underestimated. For science to provide answers to the questions concerning the equatorial sources of MSTIDs, day-to-day and seasonal source analysis of the aforementioned events had been conducted to determine the propagation directions of the various MSTIDs propagating in the region [19,20]. The most recent MSTIDs observed in summer propagated in the southeastward direction [19,20], which is poleward. They reported that those MSTIDs might have been triggered by atmospheric gravity waves that were generated during the ITCZ. The migration of the ITCZ occurs in the South American continent during summer and in the northern hemisphere during winter. Therefore, the ITCZ position is consistent with the MSTID propagation direction.

As such, we investigated the primary sources of MSTIDs over the South American equatorial region that propagated southeastward. The possible sources for the equatorial MSTIDs were be limited to the ITCZ as a possible source of the gravity waves, which leads [10,20] to the excitation of the present equatorial MSTIDs.

2. Materials and Methods

2.1. Method of Calculating MSTID Characteristics

We adopted the same method used by [19,20] to calculate the MSTID characteristics from January 2014 to December 2019. We used data from dual-frequency GNSS receivers installed in the South American low-latitude and equatorial region. We selected the area between 10° N–20° S and 30–60° W to investigate the possible source regions of the MSTIDs that propagated over the region. We also used two-dimensional dTEC maps generated with a temporal resolution of 3 min, a spatial resolution of 0.25° × 0.25°, and 5° × 5° smoothing in longitude and latitude: The color table used had a range of 0.2 to −0.4 TECU [20]. Series of dTEC maps were generated from 18:27:00 UT (15:27:00 LT) to 18:36:00 UT (15:36:00 LT) to observe the propagation of the MSTIDs in the South American region on 1 January 2017 as shown in Figure 1.

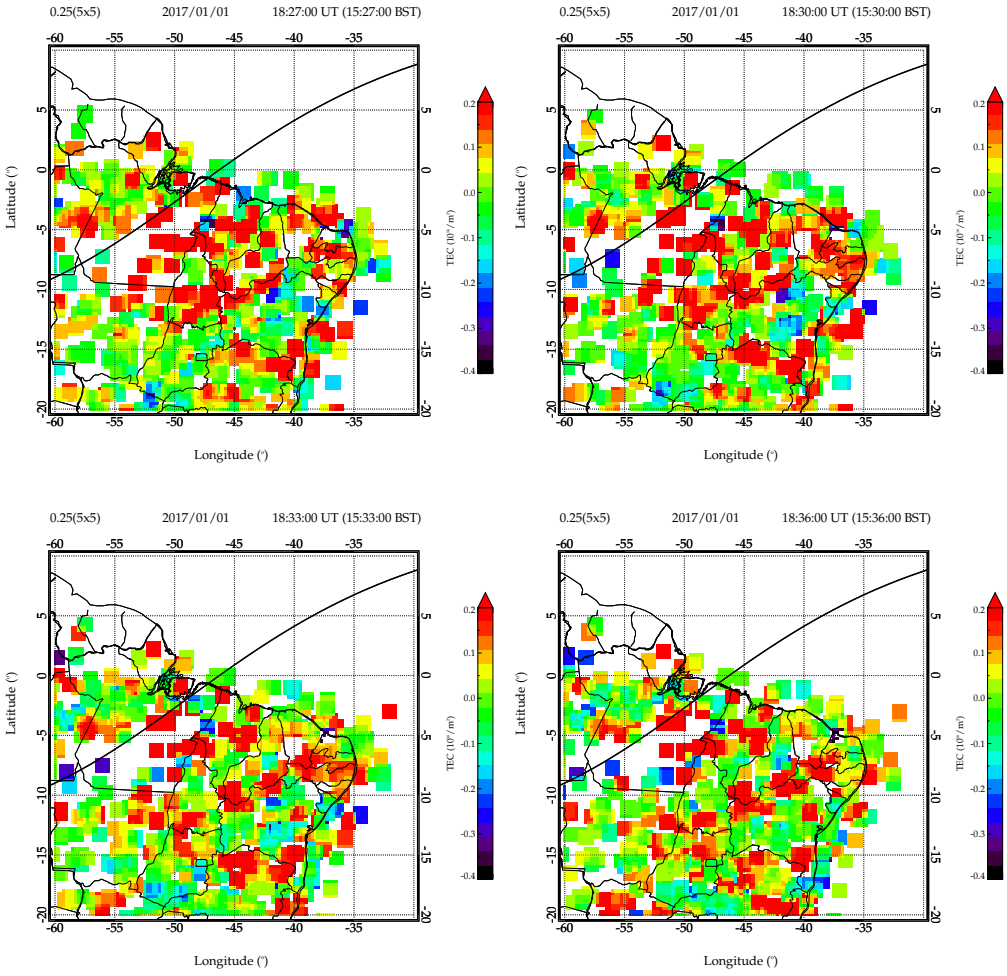

Figure 1. The series of dTEC maps on 1 January 2017 from 18:27:00 UT (15:27:00 LT) to 18:36:00 UT (15:36:00 LT) in 3 min time intervals.

We created keograms for the various dTEC maps to help identify the MSTID oscillations and their behaviors over 24 h in one single frame. For instance, we made a cut at latitude 7.5° S and longitude 35.0° W using 30 June 2015 as a case study. From the keogram, the MSTID oscillations were identified with positive (red) and negative (blue) dTEC lines denoting crests and troughs, respectively. The black dashed lines indicate the dawn and dusk solar terminator at an altitude of 300 km. The wavelength, period, direction of propagation, and phase velocity were calculated using discrete Fourier transform [19,20]. This was achieved by selecting the area of interest from the longitudinal and latitudinal keogram, as indicated by the black box shown in Figure 2.

On 1 January 2017, we calculated the characteristics of MSTID oscillations with a horizontal wavelength of 757.3 km, period of 37.7 min, and phase velocity of 335.1 m/s.

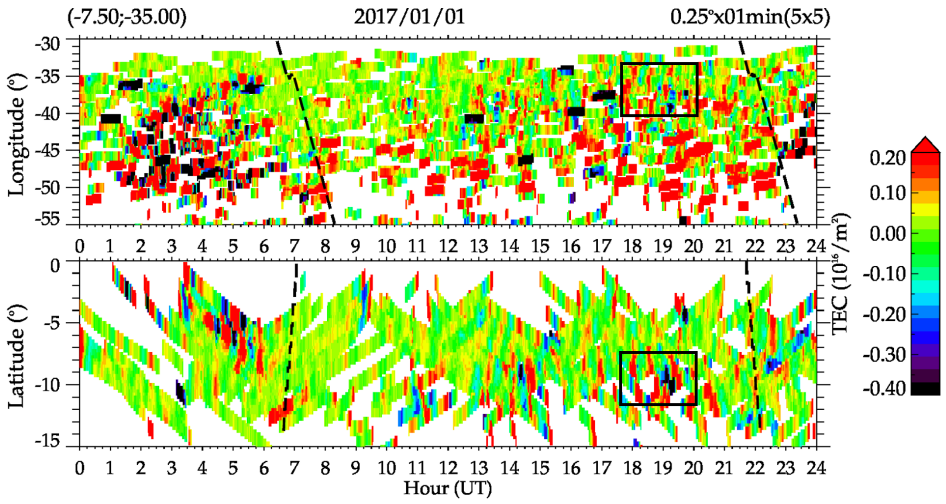

Figure 2. Keograms created from dTEC maps on 1 January 2017: longitudinal (**top**) and latitudinal (**bottom**). The black dashed lines indicate the dawn and dusk solar terminator.

2.2. Method of Identifying the ITCZ

To identify the performance and position of the ITCZ, images from Geostationary Operational Environmental Satellite (GOES) 13 and 16 were used in the infrared channel (IR) in window 10.8 µm and 11.2 µm, respectively, and water vapor (WV) in window 6.7 µm and 6.95 µm, respectively, with a horizontal resolution of 0.425° latitude × 0.425° longitude in every 30 min and 10 min, respectively. This was obtained from the Division and Environmental Systems (DSA) of the National Institute for Space Research (INPE; http://satelite.cptec.inpe.br/acervo/ (accessed on 1 July 2022). Figure 3 shows an image in the WV channel on 1 January 2017 at 12:30 UTC observed by the GOES 13 satellite.

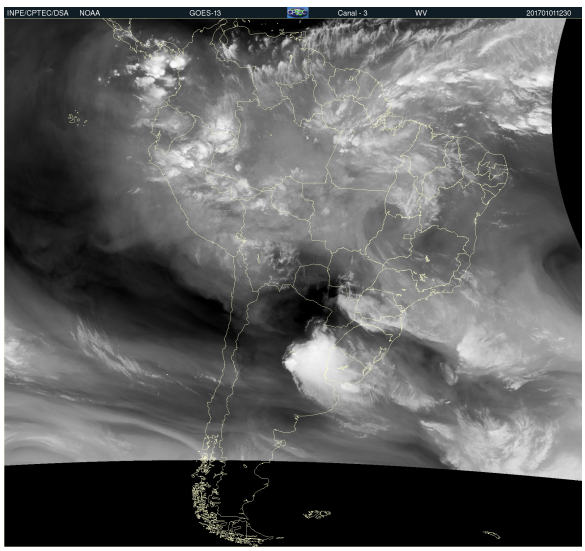

Figure 3. GOES 13 satellite image in the WV channel on 1 January 2017 at 12:30 UTC.

In addition, we obtained the variables of outgoing longwave radiation (OLR; W/m^2), the zonal and meridional wind components (m/s), the vertical velocity (omega; Pa/s), and the relative humidity (%). These reanalysis data have a horizontal resolution of 2.5° × 2.5° latitude and longitude, every 6 hours. It is supported and available by the National Centers for Environmental Predictions (NCEP) of the National Oceanic and Atmospheric

Administration (NOAA; https://psl.noaa.gov/data/gridded/ (accessed on 1 July 2022)). These data were used to generate the dynamics and thermodynamics fields of the daily averages between latitude 40° S and 20° N and longitude 90° and 20° W.

The fields composed of filtered OLR were used to obtain information related to the convective cloud [21]. The remaining fields were used for the identification of the main large-scale systems (synoptic scale) responsible for the convective activity over South America; these are the ITCZ [22,23], the high-levels cyclonic vortex (HLCV) [24], Bolivia high (BH) [25–27], South Atlantic convergence zone (SACZ) [21,28,29], and transients such as frontal systems (FSs) [30]. A brief description of these systems and their performance in different regions and seasons of the year over South America can be found in [31]. The vertical cross-sections confirmed the performance of the ITCZ, built at fixed lengths of 30–60° W and variable latitude according to the position of the ITCZ.

The ITCZ was identified in the streamline fields through the aerodynamic convergence of winds at the level of 1000 hPa (112 m: left hand side), around the parallel ~2.5° N over the ocean and <0° S over the continent, and the divergence (right side) in the tropopause at the 200 hPa level, as shown in Figure 4. Then, we validated the position of the ITCZ with a satellite image observed by GOES 13 and 16, through clusters of convective clouds at equatorial latitudes. BH and HLCV were also identified by anticyclonic and cyclonic circulation, respectively, in the horizontal fields of current lines in the tropopause [32–35]. The frontal systems that remained permanent formed a band of cloudiness in the northwest–southeast direction in the satellite images and OLR plot shown in Figures 3 and 4 respectively, in parallel with the convergence of the winds in the fields of the current lines at low levels, which we also identified as the SACZ [28,36].

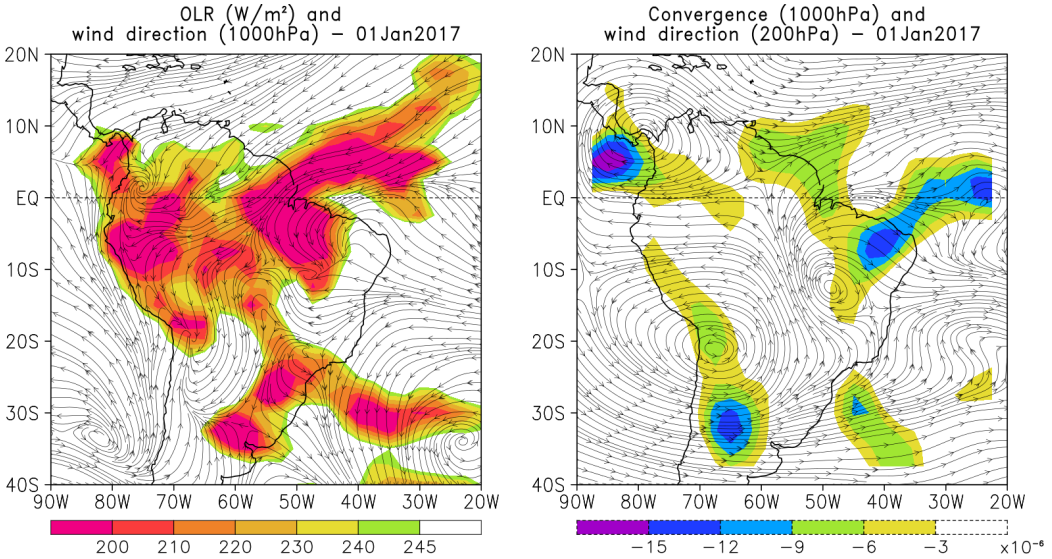

Figure 4. First panel: average daily OLR fields (shaded) and horizontal wind current at 1000 hPa (streamlines). **Second panel**: wind convergence at 1000 hPa (shaded) and horizontal wind at 200 hPa (streamlines). Both figures correspond to 1 January 2017.

The dynamic fields are composed of streamlines and omega (Pa/s) at standard levels of 1000, 925, 800, 700, 500, 300, and 200 hPa and flow divergence (1/s) at 1000 hPa; the OLR was filtered from the thermodynamics fields (OLR < 245 W/m^2). Figure 5 shows the meridional ascending humidity (%) and vertical velocity (omega (Pa/s)) in the layer between 1000 and 200 hPa, constructed in the fixed longitudinal range between 30° and 60° W and variable latitude according to the apparent position of the ITCZ in the GOES 13 image in Figure 3. These are important indicators to confirm the performance of the ITCZ through the identification of upward movements and high humidity (RH > 80%), characteristic of this system [22].

Figure 5 shows the ascending humidity and vertical velocity profiles of the from sea level to the tropopause over the tropical Atlantic Ocean between 30° and 51° W. The ascending humidity profile shows values up to ∼80% in the most intense region where the ITCZ operates over the ocean and above 90% over the continent. This day was highly humid between 45° and 30° W at the low-pressure level and extended to the tropopause. The upward vertical movements from the atmospheric layers close to the surface to the high levels is also shown by the current lines with a vertical velocity above 0.2 Pa/s. The negative sign is an indication of an ascending profile.

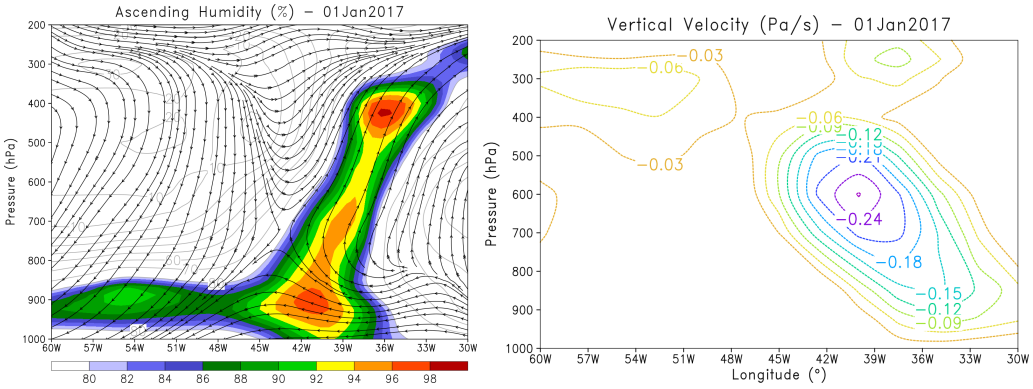

Figure 5. The ascending humidity profile and omega (Pa/s) at standard levels on 1 January 2017.

The fields described above were obtained through the following equations:

$$\frac{dx}{u} = \frac{dy}{v} \tag{1}$$

$$D = \frac{\partial u}{\partial x} + \frac{\partial v}{\partial y} \tag{2}$$

where Equation (1) is the equation of streamlines in cartesian coordinates and Equation (2) is the horizontal divergence (positive in regions of divergence and negative in regions of convergence of currents of air), where u is the zonal and v is the meridional wind component, and x and y are the latitudinal and longitudinal coordinates, respectively.

3. Results and Discussion

3.1. Characteristics of MSTIDs Propagating Southeastward

After analyzing the dTEC maps obtained by the GPS and GLONASS receivers in the South American equatorial region from January 2014 to December 2019, we observed 144 MSTIDs propagating in the southeast direction during geomagnetically quiet conditions.

Figure 6 shows the wavelength, period, phase velocity, and propagation direction of the observed MSTIDs that propagated in the southeast direction. The solid black line on the wavelength, period, and phase velocity represents the Gaussian distribution fit. The horizontal wavelengths were divided into 100 km bins, and most of them were between 500 and 800 km with a mean of 698 ± 124 km. The periods were binned into 10 min intervals and peaked between 30 and 45 min, with a mean value of 38 ± 48 min. The phase velocities of the observed MSTIDs were divided into 100 m/s bins, with the majority of them distributed between 200 and 400 m/s, with a mean distribution of 299.78 ± 89 m/s. For the propagation direction, the data were classified into 30° bins and defined as the angle clockwise from geographical north. Almost 96.5% of the MSTIDs were observed during the daytime (blue arrows); hence, the discussion was limited to the daytime MSTIDs. The horizontal wavelength, period, and phase speed of the present MSTIDs were similar to Essien et al. [20]. Moreover, we focused on the sources of the MSTIDs; hence, our concentration was limited to the propagation direction.

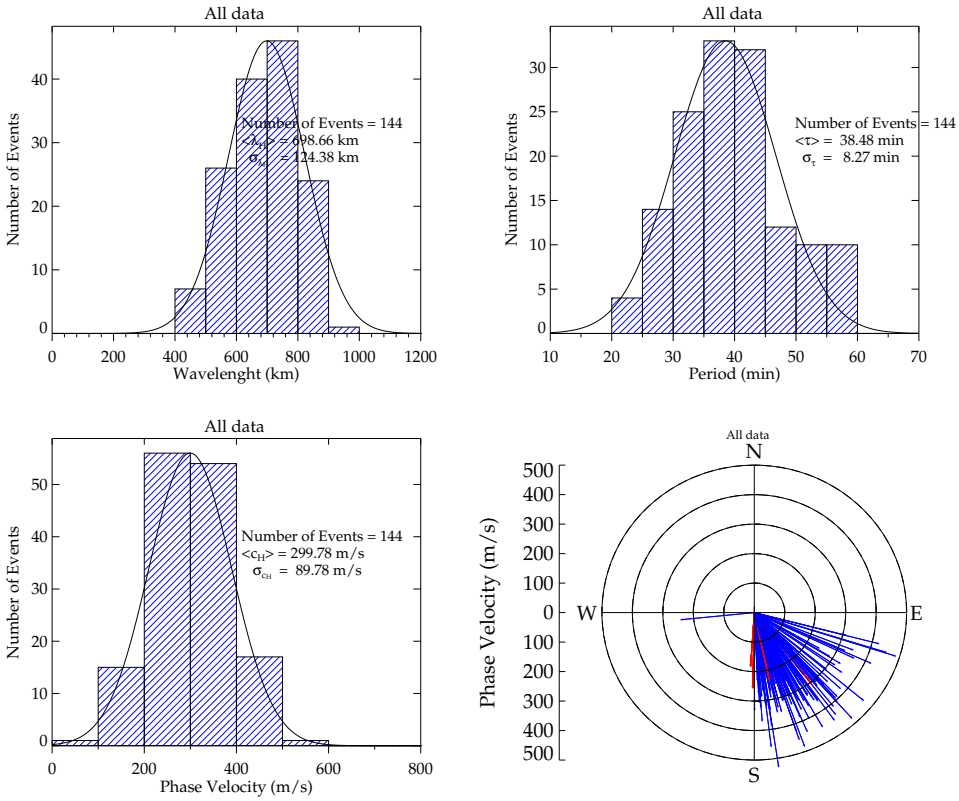

Figure 6. The wavelength, period, phase velocity, and propagation direction (red and blue arrows indicate the nighttime and daytime MSTID events, respectively) of the observed medium-scale traveling ionospheric disturbance.

3.2. Case Study of MSTIDs and ITCZ Positions

In order to relate the gravity generated by the ITCZ as the possible primary source of the MSTIDs, we plotted the MSTIDs and the ITCZ positions on the South American map, as shown in Figure 7: The first column shows the observed MSTIDs over the South American continent, with the arcs showing the concentric nature of the waves and arrows indicating the propagation direction of the MSTID oscillations. The second and third columns represent the ITCZ convergence (1000 hPa) and divergence (200 hPa) position using reanalysis data. The following days, among others, were considered for the case study of the ITCZ as the potential source of MSTIDs propagating southeastward: (a) 5 January 2016, (b) 1 January 2017, (c) 29 January 2017, and (d) 23 July 2018.

In the case of (a), (b), (c), and (d), the ITCZ was located between 0–5° S and 0–5° N, over the tropical Atlantic band, which is visible by the convergence and divergence of the winds in the equatorial latitude, as shown in column a and 3. Over the continent, however, the position of the ITCZ was below 0° S for all days, although the ITCZ position was not clear due to the mountain ranges [37]. The performance of BH as a result of superficial warming over the central part of South America and frontal systems over the southeastern region enabled the occurrence of convective activity over these regions [38]. The predominance of the performance of these systems during the day could be observed in the satellite images on the IR channel, where the frontal systems moved in the northeast direction coupled to BH during most of the day, forming a convection northwest–southeast corridor.

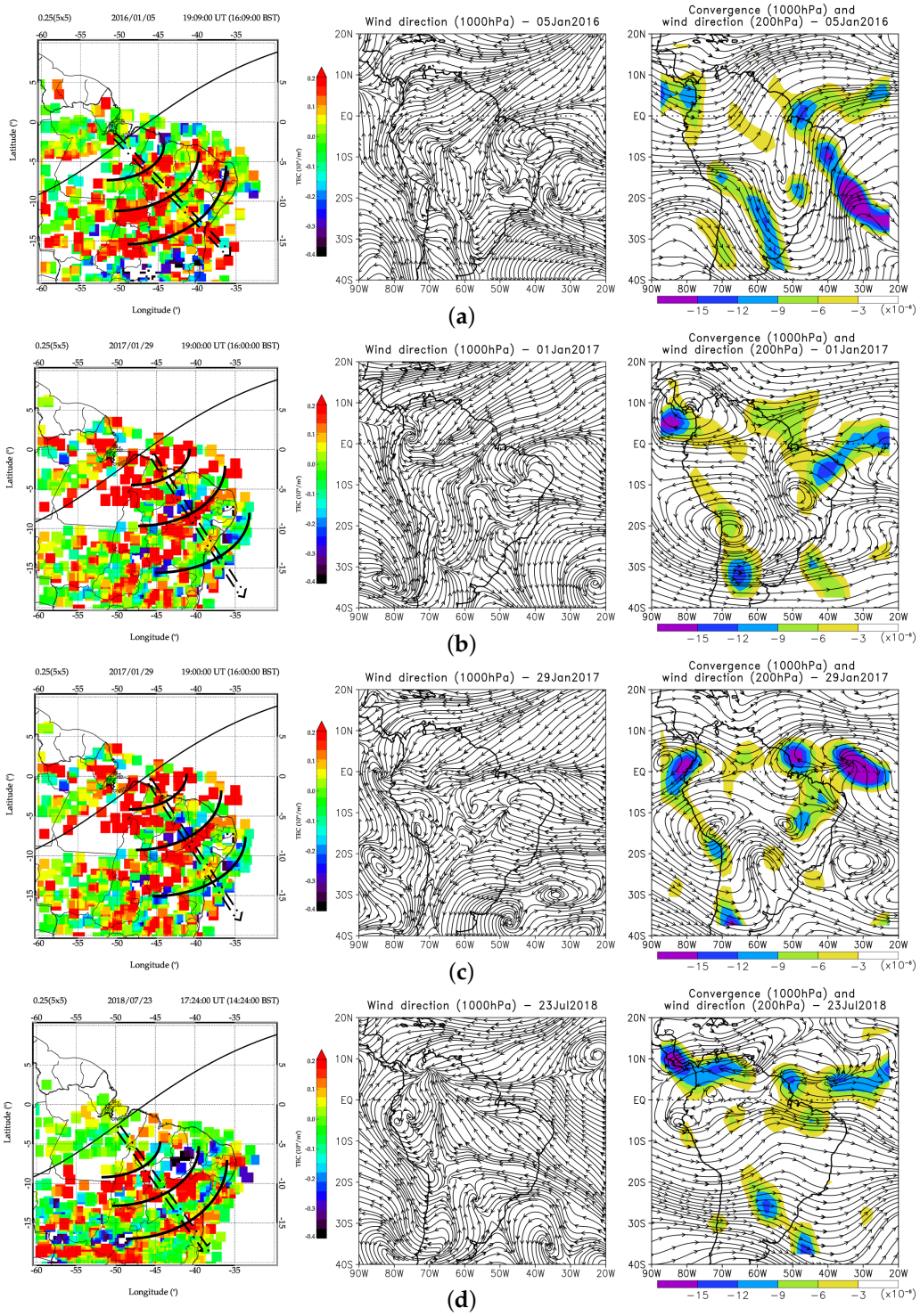

Figure 7. The ITCZ positions and the observed MSTIDs over South America on (**a**) 5 January 2016, (**b**) 1 January 2017, (**c**) 29 January 2017, and (**d**) 23 July 2018. In (**a**–**d**); the first column is the observed MSTIDs, with arcs showing the concentric nature of the waves, and the arrows showing the propagation direction; the second and third columns represent the ITCZ convergence (1000 hPa) and divergence (200 hPa) positions using reanalysis data.

The characteristics of the MSTIDs were also calculated; for instance, on the 5 January 2016, the oscillation was observed at 16:16 LT with a horizontal wavelength of 922.8 km, period of 52.0 min, and phase velocity of 295.8 m s^{-1}. On 1 January 2017, we also observed MSTID oscillations at 15:27 LT with a horizontal wavelength of 757.3 km, period of 37.7 min, and

phase velocity of 335.1 m s^{-1}. We observed another MSTID with horizontal wavelength of 751.0 km, period of 40.0 min, and phase velocity of 312.9 m s^{-1} on 29 January 2017 at 16:03 LT. Finally, the wavelength, period, and phase speed of the MSITDs observed on 23 July were 798.16 km, 42.3 min, and 314.24 m s^{-1}, respectively. These MSTID characteristics are usual in the low-latitude and equatorial regions [20].

The southeastward propagation direction of the MSTIDs in Figure 7 correlate with the corresponding ITCZ position, which is the average situation of the performance of the synoptic scale systems responsible for convective activity over the South America region. On these days, we found that MSTIDs were propagating southeastward toward the pole. This implied that the possible source positions of the MSTIDs were over the north [39–43]; hence, the propagation direction of the MSTIDs is still a strong factor for tracing the possible sources. Therefore, the ITCZ position is still the preferred candidate for the possible primary source of the observed MSTIDs propagating southeastward.

Essien et al. [20] reported that the MSTIDs propagating southeastward over the South American equatorial region might have been excited by the atmospheric gravity waves generated by the ITCZ in the troposphere. In the Peruvian equatorial region, Röttger [18] found a significant correlation with rainfall activity and the occurrence of MSTIDs. They concluded that penetrative cumulus convection in the ITCZ was the most likely mechanism generating the gravity waves exciting the observed TIDs. In the northeast of Brazil, MacDougall et al. [10] reported that the possible source of the southeastward TIDs was the ITCZ. The Spread F Experiment was performed from September to November 2005 over the South American region to define the potential role of neutral atmosphere dynamics [44]. They found that gravity waves propagating upward from the lower atmosphere were the seeding mechanism of the equatorial ESF and plasma bubbles extending to higher altitudes. For the first time, we used MSTID propagation directions as a proxy to study the source regions.

During the ALOHA-93 campaign, Gardner [45] presented aircraft-borne Michelson interferometer measurements of OH Meinel band rotational temperature and integrated band radiance observed during a trans-equatorial flight over the ITCZ. The aircraft motion afforded the opportunity to examine the horizontal wave number spectra of the gravity wave inducing fluctuations in the mesospheric OH temperature and radiance [45,46], and both showed the presence of gravity waves confined to regions near the equator. According to them, the spatial variation in the wavelength of these waves suggested that the sources were associated with the convective instabilities of the ITCZ, which implied that the ITCZ may play an important role in mesospheric circulation through its generation of gravity waves.

Vadas and Fritts [47] employed a linear model of the responses to local body forces to estimate the spectra of gravity waves arising due to vertical motions within mesoscale convective complexes (MCCs) at equatorial latitudes. They then used the ray tracing method to propagate these spectra through model wind and temperature fields and found that gravity wave forcing by MCCs was dominated by large vertical motions of limited horizontal extent, that individual convective cells within an MCC effectively acted as independent sources of gravity waves if they were separated by two or more diameters, and that vertical body forces created higher-frequency gravity waves than comparable horizontal body forces.

Since the early theories of Hines [5], Hines and Reddy [48], tropospheric phenomena, such as weather systems and the orographic lifting of air masses, have long been suspected as sources of atmospheric gravity waves. Due to the amplitude growth with increasing altitude, which offsets the decreasing atmospheric density, these waves of tropospheric origin are expected to significantly contribute to the wave energy present in the mesosphere [5,49] and subsequently ionosphere [2,3]. Additionally, gravity waves are assumed to be generated by mesoscale convective systems in the troposphere and propagate up to the F region as plasma fluctuations [5]. These mesoscale convective systems are usually

found within the ITCZ, and even ESF morphology is assumed to be controlled by the seasonal migration of gravity waves generated by the ITCZ [8,9].

The study of TID commenced in the early days of long-distance radio transmission, considering variations and interruptions in over-the-horizon transmissions [4]. In the pioneer paper published by Hines [5], TIDs were proposed to be caused by the upward propagating gravity wave disturbances originating from the neutral atmosphere (e.g., troposphere). The gravity-wave–MSTID transfer function depends on characteristics, such as period, phase velocity, horizontal wavelength, wavenumber, and amplitude and propagation direction of the wave in question, in addition to the conditions in the neutral atmosphere and ionosphere [6,7].

Investigations into the origin of the present equatorial MSTIDs from the neutral atmosphere and other geophysical sources in relation to the propagation direction are also important to science. The ITCZ produces atmospheric gravity waves in the upper troposphere to the stratosphere, and according to Hines [5], Georges and Hooke [7], Fritts et al. [44], part of these waves penetrate to the mesosphere and lower thermosphere and produce ionospheric perturbations [8,9]. For the first time, daytime MSTIDs (plasma density disturbances) propagating southeastward over the South American region were found to be excited by the passage of atmospheric gravity waves generated by ITCZ.

3.3. Seasonal Migration of ITCZ and Variations in MSTIDs Propagation Direction

Considering the seasonal average position of the ITCZ on various days, the MSTIDs observed propagating southeastward were compiled and plotted alongside the seasonal variation in the propagation directions of the correspond MSTIDs, as shown in Figure 8. Out of the 144 MSTIDs observed from January 2014 to December 2019, 20 MSTIDs were observed in winter, accounting for 13.9% of the total observations. In the equinoxes (spring and fall), 44 MSTIDs were observed, accounting for 30.6% of the entire observations. Moreover, in summer, 80 MSTIDs were observed, accounting for 55.6% of the total observations. This provided clear statistics to analyze the seasonal variability in the MSTID propagation direction with ITCZ migration. In summer, the average position of the ITCZ was located at latitude ∼0°; during the winter, it was located at ∼10° N.

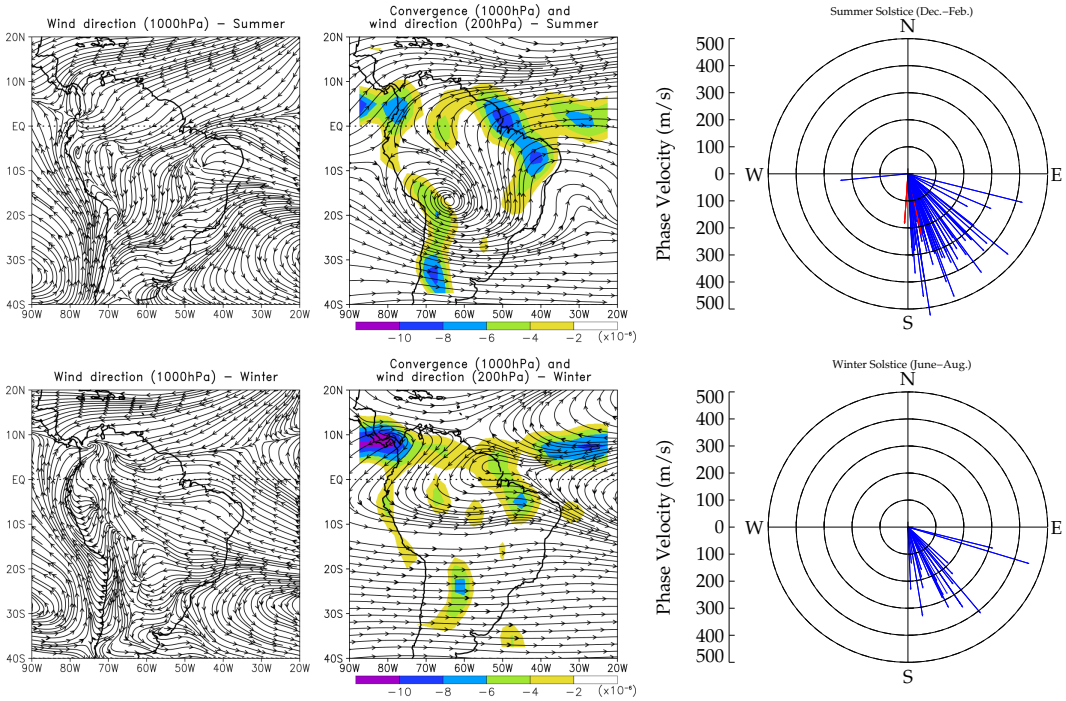

Figure 8. Seasonal average position of the ITCZ (first two columns) and propagation direction of the observed MSTIDs (third column).

For the first time, we identified the relationship between the ITCZ position and the MSTIDs propagating in the southeast direction. We found that the frequency of the occurrence of MSTIDs propagating in the southeast direction in summer was much higher than that in winter, which is contrary to the statistics reported by Figueiredo et al. [19], Essien et al. [20] in the same region. This implies that the frequency at which MSTIDs occur in a particular region depends on the possible mechanism that triggers them. The present seasonal variation in the occurrence of MSTIDs propagating southeastward could be explained by the seasonal migration of the ITCZ, as shown in the first column of Figure 8. In winter, the ITCZ lies to the north of the equator, between 10° to 15° N, which resulted in the fewer observations of MSTIDs propagating southeastward. In summer, the ITCZ migrated into the southern hemisphere between 0° and 5° S over the continent, which consequently triggered more MSTIDs propagating southeastward [50]. The present results explain why the southeastward MSTIDs reported in previous studies [19,20] are rare in equatorial and low-latitude regions during winter and dominant in summer.

The ITCZ is characterized by low atmospheric pressures due to the upward movement induced by the trade winds from the Northern and Southern Hemisphere convergence, which results in high atmospheric pressure in the upper troposphere [51]. This permanent low-pressure feature lies in the equatorial trough, where surface trade winds laden with heat and moisture converge to form a zone of increased convection, cloudiness, and precipitation [50] and, consequently, rainfall [52]. These are all sources of atmospheric gravity waves in the troposphere [40], which propagate vertically upward in the ionospheric level as plasma fluctuations [5,8,9,20].

Ref. [52] reported from paleoclimatic studies that changes in the tropical rainbelt across the Atlantic Ocean during the past two millennia have been linked to a latitudinal shift of the intertropical convergence zone (ITCZ) driven by the Northern Hemisphere (NH) climate. The latent heat released in the ITCZ is critical to the atmospheric energy budget, and ITCZ cloudiness provides an important contribution to the planetary albedo: the position, structure, and migration of the ITCZ influence ocean/atmosphere and land/atmosphere interactions on a global scale. The resulting circulation that forms with air converging near the surface around the equator and diverging above is known as the Hadley Cell [53]. Throughout the year, the ITCZ follows the migration of the Sun's overhead position, typically with a delay of around 1–2 months. As the ocean more slowly heats up than land, the ITCZ tends to move further north and south over land areas than over water. In winter, the ITCZ lies well to the north of the equator and migrates to the south in summer [50].

The deep convective field shows an intense convection signal over the South American equatorial region during summer and autumn/fall as a result of surface warming, and BH at ∼5° S. During spring, the convective activity is weak in the equatorial region but intense in the southeast and subtropical latitudes between 25° and 40° S. Most of the MSTIDs propagating southeastward have high phase velocity, equivalent to the phase speed of secondary and tertiary waves [54]. Therefore, it is also possible that some of the MSTIDs in the present study might have been excited by secondary and tertiary gravity waves that were generated from the ITCZ.

In order to study the local time variations in the MSTIDs that propagated southeastward over the South American region, we plotted the occurrence rate in azimuth and hourly bins, as shown in Figure 9. In summer, the MSTIDs that propagated southeastward occurred between 16:00 and 23:00 UT (13:00–20:00 LT), with a minor peak in the evening between 18:00 and 23:00 UT (15:00–20:00 LT). During winter, almost all the MSTIDs propagating southeastward occurred during daytime between 12:00 and 20:00 UT (09:00–17:00 LT). The occurrence rate was classified into daytime (7:00–17:00 LT), evening (17:00–20:00 LT), and nighttime (21:00–4:00). In summer, most of the MSTIDs had azimuthal values between 150° and 180°, which occurred during evening, with few between 120° and 150° occurring during the day. It should be noted that the azimuthal values of the MSTIDs that might be triggered by the ITCZ strongly depend on the local time, as clearly shown in the seasonality of their local time dependence.

The ITCZ provides a useful framework to study the primary source region of the gravity waves that might propagate to the ionospheric level as MSTIDs. In the this study, we investigated the MSTIDs propagating in southeast direction and the ITCZ, which is suspected to be the possible primary source. The source region with respect to the propagation direction is an important factor to consider to identify the MSTID source regions [40]. The anisotropy observed in the propagation direction of the present MSTIDs could be due to the position and migration of the ITCZ MacDougall et al. [10], Röttger [18], Essien et al. [20]. MSTIDs have been known to constitute a specific type of space weather and geophysical phenomenon that can be solar-driven or driven by other processes from auroral sources in the high-latitude thermosphere to the solar terminator and storms, tropospheric convection, hurricanes, and tornadoes in the troposphere [15,55].

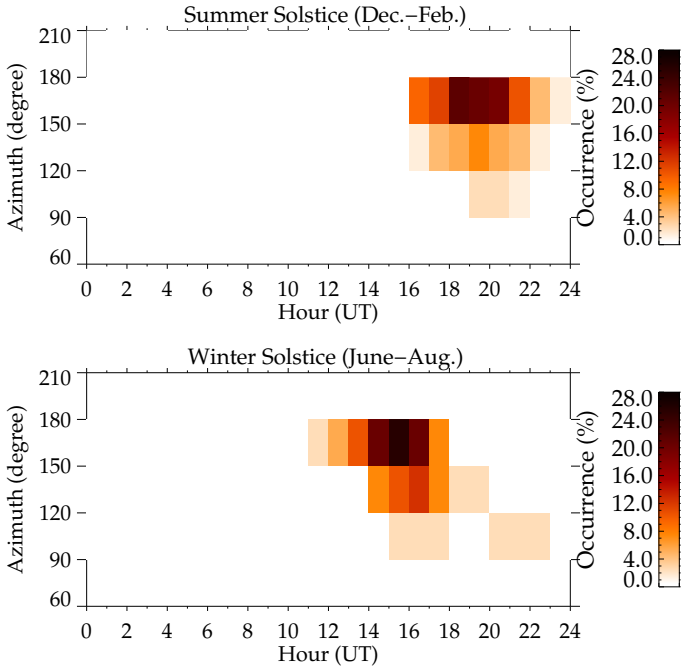

Figure 9. Time dependence of and seasonal variation in the occurrence of MSTIDs propagating southeastward over the South American equatorial region between January 2014 and December 2019.

4. Conclusions

Using the data collected by the GNSS dual-frequency receivers network, detrended TEC maps were generated to identify and characterize medium-scale traveling ionospheric disturbances (MSTIDs) propagating in the southeast direction over the South American region from January 2014 to December 2019. To study the sources of the observed MSTIDs, we used images from the Geostationary Operational Environmental Satellite (GOES) 13 and 16 in the infrared (IR; 10.8 µm and 11.2 µm, respectively) and water vapor (WV; 6.7 µm and 6.95 µm, respectively) channels, with a horizontal resolution of latitude 0.425° × longitude 0.425° every 30 min, and reanalysis data with a horizontal resolution of latitude 2.5° × longitude 2.5° for every 6 h, to study the daily features and seasonal migration of the ITCZ.

- The propagation direction of a total of 144 MSTIDs was observed during the days the ITCZ was active, and the statistical analysis of the seasonal variability of the MSTIDs was thoroughly recorded. We found that in the winter and equinoxes, 20 and 44 MSTIDs were observed, respectively. Moreover, in summer, 80 MSTIDs were observed propagating southeastward.
- The seasonal variation in the occurrence of the observed MSTIDs propagating to the southeast direction coincided with the ITCZ occurrences. The ITCZ lies to the north of the equator, between 10° and 15° N during winter, which decreased the occurrence

of MSTIDs propagating southeastward. However, in summer, the ITCZ migrated to the Southern Hemisphere (0° to 5° S), which triggered more MSTIDs propagating southeastward.

- In the winter, when the ITCZ migrates to the Northern Hemisphere between 10° N and 15° N, 20 MSTIDs propagated southeastward. We realized that during summer when the ITCZ lies within the continent, between 0° S and 5° S, 80 MSTIDs were observed propagating southeastward.
- We found and showed for the first time that the day-to-day observation of the ITCZ position and MSTID propagation directions are consistent.
- With regard to the above new findings, we report that the MSTIDs propagating southeastward over the South American region are induced by the atmospheric gravity waves generated by the ITCZ in the troposphere.
- We also discovered that the MSTIDs propagating southeastward show a clear seasonality of their local time dependence. In summer, the MSTIDs frequently occurred in the evening hours; those in winter occurred during the daytime.
- The mean of the horizontal wavelength, period, and phase velocity were 698 $\pm$ 124 km, 38 $\pm$ 8 min, and 299 $\pm$ 89 m s^{-1}, respectively.

Author Contributions: Conceptualization, P.E., H.T., C.M.W., T.T.A., J.H.A.S., D.B. and A.V.B.; Data curation, C.A.O.B.F. and C.M.W.; Formal analysis, P.E., C.A.O.B.F., C.M.W. and J.M.d.S.A.; Funding acquisition, N.A.B.K.; Investigation, P.E., C.A.O.B.F., C.M.W. and J.M.d.S.A.; Methodology, P.E., C.A.O.B.F., H.T., C.M.W., J.M.d.S.A., D.P.Q., S.O.L., D.B., A.V.B., F.N. and K.A.Q.; Resources, P.E.; Software, C.A.O.B.F.; Supervision, H.T.; Visualization, P.E.; Writing—original draft, P.E., C.A.O.B.F., H.T., N.A.B.K., D.P.Q., T.T.A., J.H.A.S., M.J.E., S.S.S., A.V.B., F.N. and K.A.Q.; Writing—review & editing, P.E., C.A.O.B.F., H.T., N.A.B.K., C.M.W., J.M.d.S.A., S.O.L., J.H.A.S., M.J.E. and S.S.S. All authors have read and agreed to the published version of the manuscript.

Funding: This research is funded by African Institute for Mathematical Sciences (AIMS) Rwanda. Also, Nacional de Desenvolvimento Cientifico e Tecnologico (CNPq), project no. 141044/2017-9 and Coordenacao de Aperfeicoamento de Pessoal de Nivel Superior (CAPES) contributed for the data processing and analysis.

Data Availability Statement: The data used in this paper can be access from the official website of the RMBC, RAMSAC, LISN, IGS, GOES and NOAA.

Acknowledgments: We thank the African Institute for Mathematical Sciences (AIMS) Rwanda, Climate science, for providing the required resources for this work. We thank all the institutes that own the GNSS receivers network over South America: RBMC (Brazilian Institute of Geography and Statistics, Brazil), RAMSAC (National Geographic Institute, Argentina), CORS (National Geodetic Survey, USA), IGS (International GNSS Service), and UNAVCO (National Science Foundation, USA and National Atmospheric and Space Administration, USA), for making available the RINEXs files, which were important for obtaining the results. We are grateful to the Brazilian Space Climate Study and Monitoring program (EMBRACE) for making RINEX files available. We thank the Center for Weather Forecasting and Climate Studies (CPTEC) for providing images from the Geostationary Operational Environmental Satellite (GOES). C.A.O.B.F. thanks the Fundação de Amparo à Pesquisa do Estado de São Paulo (FAPESP) under the process 2018/09066-8 and 2019/22548-4, and the National Institute for Space Research (INPE). We also thank National Centers for Environmental Predictions (NCEP) of the National Oceanic and Atmospheric Administration (NOAA) for the reanalysis data and the Division and Environmental Systems (DSA) of the National Institute for Space Research (INPE) for the Geostationary Operational Environmental Satellite (GOES) 13 and 16.

Conflicts of Interest: The authors of this current work, solemnly declare no conflict of interest as far as the entire work is concerned.

References

1. Astafyeva, E. Ionospheric Detection of Natural Hazards. *Rev. Geophys.* **2019**, *57*, 1265–1288. [CrossRef]
2. Abdu, M.A.; Kherani, E.A.; Batista, I.S.; de Paula, E.R.; Fritts, D.C.; Sobral, J.H.A. Gravity wave initiation of equatorial spread F/plasma bubble irregularities based on observational data from the SpreadFEx campaign. *Ann. Geophys.* **2009**, *27*, 2607–2622. [CrossRef]

3. Earle, G.D.; Musumba, A.M.; Vadas, S.L. Satellite-based measurements of gravity wave-induced midlatitude plasma density perturbations. *J. Geophys. Res. Space Phys.* **2008**, *113*. [CrossRef]
4. Crowley, G.; Azeem, I. Extreme Ionospheric Storms and Their Effects on GPS Systems. In *Extreme Events in Geospace*; Elsevier: Amsterdam, The Netherlands, 2018; pp. 555–586.
5. Hines, C.O. Internal atmospheric gravity waves at ionospheric heights. *Can. J. Phys.* **1960**, *38*, 1441–1481. [CrossRef]
6. Hooke, W.H. Ionospheric irregularities produced by internal atmospheric gravity waves. *J. Atmos. Terr. Phys.* **1968**, *30*, 795–823. [CrossRef]
7. Georges, T.M.; Hooke, W.H. Wave-induced fluctuations in ionospheric electron content: A model indicating some observational biases. *J. Geophys. Res.* **1970**, *75*, 6295–6308. [CrossRef]
8. Tsunoda, R.T. On seeding equatorial spread F: Circular gravity waves. *Geophys. Res. Lett.* **2010**, *37*. 2010GL043422. [CrossRef]
9. Su, S.Y.; Wu, C.L.; Liu, C.H. Correlation between the global occurrences of ionospheric irregularities and deep atmospheric convective clouds in the intertropical convergence zone (ITCZ). *Earth Planets Space* **2014**, *66*, 134. [CrossRef]
10. MacDougall, J.; Abdu, M.A.; Batista, I.; Buriti, R.; Medeiros, A.F.; Jayachandran, P.T.; Borba, G. Spaced transmitter measurements of medium scale traveling ionospheric disturbances near the equator. *Geophys. Res. Lett.* **2011**, *38*. [CrossRef]
11. Otsuka, Y.; Suzuki, K.; Nakagawa, S.; Nishioka, M.; Shiokawa, K.; Tsugawa, T. GPS observations of medium-scale traveling ionospheric disturbances over Europe. *Ann. Geophys.* **2013**, *31*, 163–172. [CrossRef]
12. Paulino, I.; Medeiros, A.F.; Vadas, S.L.; Wrasse, C.M.; Takahashi, H.; Buriti, R.A.; Leite, D.; Filgueira, S.; Bageston, J.V.; Sobral, J.H.A.; Gobbi, D. Periodic waves in the lower thermosphere observed by OI630 nm airglow images. *Ann. Geophys.* **2016**, *34*, 293–301. [CrossRef]
13. Figueiredo, C.; Takahashi, H.; Wrasse, C.M.; Otsuka, Y.; Shiokawa, K.; Barros, D. Investigation of Nighttime MSTIDS Observed by Optical Thermosphere Imagers at Low Latitudes: Morphology, Propagation Direction, and Wind Filtering. *J. Geophys. Res. Space Phys.* **2018**, *123*, 7843–7857. [CrossRef]
14. Otsuka, Y.; Kotake, N.; Shiokawa, K.; Ogawa, T.; Tsugawa, T.; Saito, A. Statistical study of medium-scale traveling ionospheric disturbances observed with a GPS receiver network in Japan. In *Aeronomy of the Earth's Atmosphere and Ionosphere*; Abdu, M.A., Pancheva, D., Eds.; Springer: Dordrecht, The Netherlands, 2011; pp. 291–299.
15. Kotake, N.; Otsuka, Y.; Ogawa, T.; Tsugawa, T.; Saito, A. Statistical study of medium-scale traveling ionospheric disturbances observed with the GPS networks in Southern California. *Earth Planets Space* **2007**, *59*, 95–102. [CrossRef]
16. Kelley, M.C.; Makela, J.J.; Saito, A.; Aponte, N.; Sulzer, M.; González, S.A. On the electrical structure of airglow depletion/height layer bands over Arecibo. *Geophys. Res. Lett.* **2000**, *27*, 2837–2840. [CrossRef]
17. Liu, Y.; Li, Z.; Fu, L.; Wang, J.; Zhang, C. Studying the ionospheric responses induced by a geomagnetic storm in September 2017 with multiple observations in America. *GPS Solut.* **2020**, *24*, 3. [CrossRef]
18. Röttger, J. Travelling disturbances in the equatorial ionosphere and their association with penetrative cumulus convection. *J. Atmos. Terr. Phys.* **1977**, *39*, 987–998. [CrossRef]
19. Figueiredo, C.; Takahashi, H.; Wrasse, C.M.; Otsuka, Y.; Shiokawa, K.; Barros, D. Medium-scale traveling ionospheric disturbances observed by detrended total electron content maps over Brazil. *J. Geophys. Res. Space Phys.* **2018**, *123*, 2215–2227. [CrossRef]
20. Essien, P.; Figueiredo, C.A.O.B.; Takahashi, H.; Wrasse, C.M.; Barros, D.; Klutse, N.A.B.; Lomotey, S.O.; Ayorinde, T.T.; Gobbi, D.; Bilibio, A.V. Long-term study on medium-scale traveling ionospheric disturbances observed over the South American Equatorial Region. *Atmosphere* **2021**, *12*, 1409. [CrossRef]
21. Kousky, V.E. Pentad outgoing longwave radiation climatology for the South American sector. *Rev. Bras. Meteorol.* **1988**, *3*, 217–231.
22. Hastenrath, S.; Greischar, L. The monsoonal current regimes of the tropical Indian Ocean: Observed surface flow fields and their geostrophic and wind-driven components. *J. Geophys. Res. Ocean.* **1991**, *96*, 12619–12633. [CrossRef]
23. Gan, M.A.; Kousky, V.; Ropelewski, C. The South America monsoon circulation and its relationship to rainfall over west-central Brazil. *J. Clim.* **2004**, *17*, 47–66. [CrossRef]
24. Kousky, V.E.; Alonso Gan, M. Upper tropospheric cyclonic vortices in the tropical South Atlantic. *Tellus* **1981**, *33*, 538–551. [CrossRef]
25. Silva, V.B.; Kousky, V.E. The South American monsoon system: Climatology and variability. *Mod. Climatol.* **2012**, *123*, 152.
26. DeMaria, M. Linear response of a stratified tropical atmosphere to convective forcing. *J. Atmos. Sci.* **1985**, *42*, 1944–1959. [CrossRef]
27. Figueroa, S.N.; Satyamurty, P.; Da Silva Dias, P.L. Simulations of the summer circulation over the South American region with an eta coordinate model. *J. Atmos. Sci.* **1995**, *52*, 1573–1584. [CrossRef]
28. Kodama, Y. Large-scale common features of subtropical precipitation zones (the Baiu frontal zone, the SPCZ, and the SACZ) Part I: Characteristics of subtropical frontal zones. *J. Meteorol. Soc. Jpn. Ser. II* **1992**, *70*, 813–836. [CrossRef]
29. Lenters, J.D.; Cook, K.H. Simulation and diagnosis of the regional summertime precipitation climatology of South America. *J. Clim.* **1995**, *8*, 2988–3005. [CrossRef]
30. Kousky, V.E. Frontal influences on northeast Brazil. *Mon. Weather. Rev.* **1979**, *107*, 1140–1153. [CrossRef]
31. Reboita, M.S.; Gan, M.A.; Rocha, R.P.d.; Ambrizzi, T. Regimes de precipitação na América do Sul: Uma revisão bibliográfica. *Rev. Bras. Meteorol.* **2010**, *25*, 185–204. [CrossRef]
32. Gutman, G.J.; Schwerdtfeger, W. The role of latent and sensible heat for the development of a high pressure system over the subtropical Andes. *Meteorol. Rundsch.* **1965**, *18*.

33. Virji, H. A preliminary study of summertime tropospheric circulation patterns over South America estimated from cloud winds. *Mon. Weather Rev.* **1981**, *109*, 599–610. [CrossRef]
34. Lenters, J.D.; Cook, K.H. On the origin of the Bolivian high and related circulation features of the South American climate. *J. Atmos. Sci.* **1997**, *54*, 656–678. [CrossRef]
35. Vuille, M. Atmospheric circulation over the Bolivian Altiplano during dry and wet periods and extreme phases of the Southern Oscillation. *Int. J. Climatol. J. R. Meteorol. Soc.* **1999**, *19*, 1579–1600. [CrossRef]
36. Quadro, M.F.L.d. Estudo de episódios de Zona de Convergência do Atlântico Sul (ZCAS) sobre a América do sul. Master's Thesis, INPE, São José dos Campos, Brazil, 1994; 99p.
37. Hastenrath, S.; Lamb, P. On the dynamics and climatology of surface flow over the equatorial oceans. *Tellus* **1978**, *30*, 436–448. [CrossRef]
38. Horel, J.D.; Hahmann, A.N.; Geisler, J.E. An investigation of the annual cycle of convective activity over the tropical Americas. *J. Clim.* **1989**, *2*, 1388–1403. [CrossRef]
39. Waldock, J.; Jones, T. Source regions of medium scale travelling ionospheric disturbances observed at mid-latitudes. *J. Atmos. Terr. Phys.* **1987**, *49*, 105–114. [CrossRef]
40. Essien, P.; Paulino, I.; Wrasse, C.M.; Campos, J.A.V.; Paulino, A.R.; Medeiros, A.F.; Buriti, R.A.; Takahashi, H.; Agyei-Yeboah, E.; Lins, A.N. Seasonal characteristics of small-and medium-scale gravity waves in the mesosphere and lower thermosphere over the Brazilian equatorial region. In *Annales Geophysicae*; Copernicus GmbH: Gottingen, Germany, 2018; Volume 36, pp. 899–914.
41. Takahashi, H.; Wrasse, C.; Figueiredo, C.; Barros, D.; Paulino, I.; Essien, P.; Abdu, M.; Otsuka, Y.; Shiokawa, K. Equatorial plasma bubble occurrence under propagation of MSTID and MLT gravity waves. *J. Geophys. Res. Space Phys.* **2020**, *125*, e2019JA027566. [CrossRef]
42. Takahashi, H.; Essien, P.; Figueiredo, C.; Wrasse, C.; Barros, D.; Abdu, M.; Otsuka, Y.; Shiokawa, K.; Li, G. Multi-instrument study of longitudinal wave structures for plasma bubble seeding in the equatorial ionosphere. *Earth Planet. Phys.* **2021**, *5*, 368–377. [CrossRef]
43. Perrett, J.A.; Wright, C.J.; Hindley, N.P.; Hoffmann, L.; Mitchell, N.J.; Preusse, P.; Strube, C.; Eckermann, S.D. Determining Gravity Wave Sources and Propagation in the Southern Hemisphere by Ray-Tracing AIRS Measurements. *Geophys. Res. Lett.* **2021**, *48*, e2020GL088621. [CrossRef]
44. Fritts, D.C.; Wang, L.; Werne, J.; Lund, T.; Wan, K. Gravity wave instability dynamics at high Reynolds numbers. Part I: Wave field evolution at large amplitudes and high frequencies. *J. Atmos. Sci.* **2009**, *66*, 112–1148. [CrossRef]
45. Gardner, C.S. Introduction to ALOHA/ANLC-93: The 1993 airborne lidar and observations of the Hawaiian airglow/airborne noctilucent cloud campaigns. *Geophys. Res. Lett.* **1995**, *22*, 2789–2792. [CrossRef]
46. Qian, J.; Gu, Y.Y.; Papen, G.C.; Gardner, C.S.; Espy, P.J. Horizontal wave number spectra of density and temperature perturbations in the mesosphere measured during the 4 August flight of ANLC-93. *Geophys. Res. Lett.* **1995**, *22*, 2865–2868. [CrossRef]
47. Vadas, S.L.; Fritts, D.C. Thermospheric responses to gravity waves arising from mesoscale convective complexes. *J. Atmos. Sol.-Terr. Phys.* **2004**, *66*, 781–804. [CrossRef]
48. Hines, C.O.; Reddy, C.A. On the propagation of atmospheric gravity waves through regions of wind shear. *J. Geophys. Res.* **1967**, *72*, 1015–1034. [CrossRef]
49. Gossard, E.E. Vertical flux of energy into the lower ionosphere from internal gravity waves generated in the troposphere. *J. Geophys. Res.* **1962**, *67*, 745–757. [CrossRef]
50. Waliser, D.; Jiang, X. *Tropical Meteorology and Climate: Intertropical Convergence Zone*; Elsevier: Amsterdam, The Netherlands, 2015.
51. Giresse, P. *Tropical and Sub-Tropical West Africa-Marine and Continental Changes during the Late Quaternary*; Elsevier: Amsterdam, The Netherlands, 2007.
52. Utida, G.; Cruz, F.W.; Etourneau, J.; Bouloubassi, I.; Schefuß, E.; Vuille, M.; Novello, V.F.; Prado, L.F.; Sifeddine, A.; Klein, V.; et al. Tropical South Atlantic influence on Northeastern Brazil precipitation and ITCZ displacement during the past 2300 years. *Sci. Rep.* **2019**, *9*, 1698. [CrossRef]
53. Madden, R.A. Tropical Meteorology and Climate: Intraseasonal Oscillation (Madden-Julian Oscillation). In *Encyclopedia of Atmospheric Sciences*; Elsevier: Amsterdam, The Netherlands, 2015; pp. 132–136.
54. Vadas, S.L.; Becker, E. Numerical modeling of the generation of tertiary gravity waves in the mesosphere and thermosphere during strong mountain wave events over the Southern Andes. *J. Geophys. Res. Space Phys.* **2019**, *124*, 7687–7718. [CrossRef]
55. Hernandez-Pajares, M.; Juan, J.M.; Sanz, J. Medium-scale traveling ionospheric disturbances affecting GPS measurements: Spatial and temporal analysis. *J. Geophys. Res. Space Phys.* **2006**, *111*. [CrossRef]